Annu. Rev. Biochem. 1998. 67:693–720

ENZYMATIC TRANSITION STATES AND TRANSITION STATE ANALOG DESIGN

Vern L. Schramm
Department of Biochemistry, Albert Einstein College of Medicine of Yeshiva University, Bronx, New York 10461; email: vern@aecom.yu.edu

KEY WORDS: catalysis, isotope effects, inhibitor, enzymes, inhibitor design

ABSTRACT

All chemical transformations pass through an unstable structure called the transition state, which is poised between the chemical structures of the substrates and products. The transition states for chemical reactions are proposed to have lifetimes near 10^{-13} sec, the time for a single bond vibration. No physical or spectroscopic method is available to directly observe the structure of the transition state for enzymatic reactions. Yet transition state structure is central to understanding catalysis, because enzymes function by lowering activation energy. An accepted view of enzymatic catalysis is tight binding to the unstable transition state structure. Transition state mimics bind tightly to enzymes by capturing a fraction of the binding energy for the transition state species. The identification of numerous transition state inhibitors supports the transition state stabilization hypothesis for enzymatic catalysis. Advances in methods for measuring and interpreting kinetic isotope effects and advances in computational chemistry have provided an experimental route to understand transition state structure. Systematic analysis of intrinsic kinetic isotope effects provides geometric and electronic structure for enzyme-bound transition states. This information has been used to compare transition states for chemical and enzymatic reactions; determine whether enzymatic activators alter transition state structure; design transition state inhibitors; and provide the basis for predicting the affinity of enzymatic inhibitors. Enzymatic transition states provide an understanding of catalysis and permit the design of transition state inhibitors. This article reviews transition state theory for enzymatic reactions. Selected examples of enzymatic transition states are compared to the respective transition state inhibitors.

0066-4154/98/0701-0693$08.00

CONTENTS

INTRODUCTION

Enzymes catalyze chemical reactions at rates that are astounding relative to uncatalyzed chemistry at the same conditions. Typical enzymatic rate enhancements are 10^{10} to 10^{15}, accomplishing in 1 sec that which would require 300 to 30,000,000 years in the absence of enzymes (1). Each catalytic event requires a minimum of three or often more steps, all of which occur within the few milliseconds that characterize typical enzymatic reactions. According to transition state theory, the smallest fraction of the catalytic cycle is spent in the most important step, that of the transition state. However, this step cannot occur without participation of the enzymatic forces that occur as the Michaelis complex is transformed into the transition state by precise alignment of catalytic groups by enzymatic and substrate conformational changes (Figure 1).

The original proposals of absolute reaction rate theory for chemical reactions defined the transition state as a distinct species in the reaction coordinate that determined the absolute reaction rate (2). Soon thereafter, Linus Pauling proposed that the powerful catalytic action of enzymes could be explained by specific tight binding to the transition state species (3). Because reaction rate is proportional to the fraction of the reactant in the transition state complex, the enzyme was proposed to increase the concentration of the reactive species. This proposal was formalized by Wolfenden and coworkers, who hypothesized that the rate increase imposed by enzymes is proportional to the affinity of

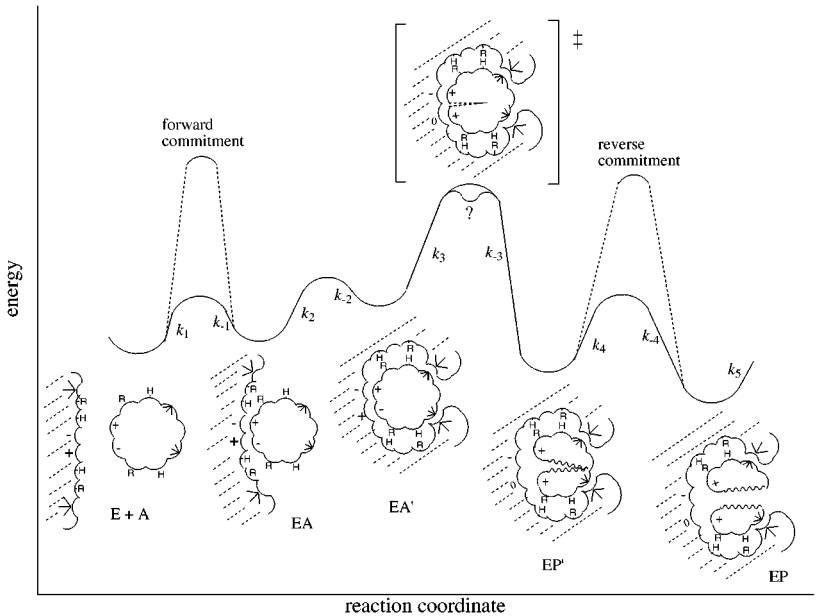

Figure 1 Reaction coordinate diagram for conversion of substrate (A) to enzyme-bound products (EP). Symbols are R = H-bond acceptor, H = H-bond donor, + and − are ionic charges, and > represents hydrophobic sites. The *solid line* is an example of fully rate-limiting transition state formation, providing intrinsic kinetic isotope effects. The energetic barriers (*dashed lines*) labeled "forward commitment" and "reverse commitment" make substrate binding and/or product release rate limiting and suppress kinetic isotope effects. The transition state has unique properties of charge and optimal H-bond alignment not found in any of the reactant species. In this example, charge repulsion serves to clear the catalytic site and restore the enzyme to the open form (E) after k_5.

the enzyme for the transition state structure relative to the Michaelis complex (4; Figure 2). Because enzymes typically increase the noncatalyzed reaction rate by factors of 10^{10}–10^{15}, and Michaelis complexes often have dissociation constants in the range of 10^{-3}–10^{-6} M, it is proposed that transition state complexes are bound with dissociation constants in the range of 10^{-14}–10^{-23} M. Analogs that resemble the transition state structures should therefore provide the most powerful noncovalent inhibitors known, even if only a small fraction of the transition state energy is captured.

Reviews from 1976, 1988, and 1995 listed enzymes known to interact with transition state inhibitors, defined as tight binding inhibitors that resemble the hypothetical transition states or intermediates for various enzymes (5–7). Between 1988 and 1995, the list grew from 33 to 132 enzymes. In 1976 and 1988, most of the inhibitors were natural products. The 1995 list of enzymes and transition state inhibitors is dominated by intentionally synthesized inhibitors

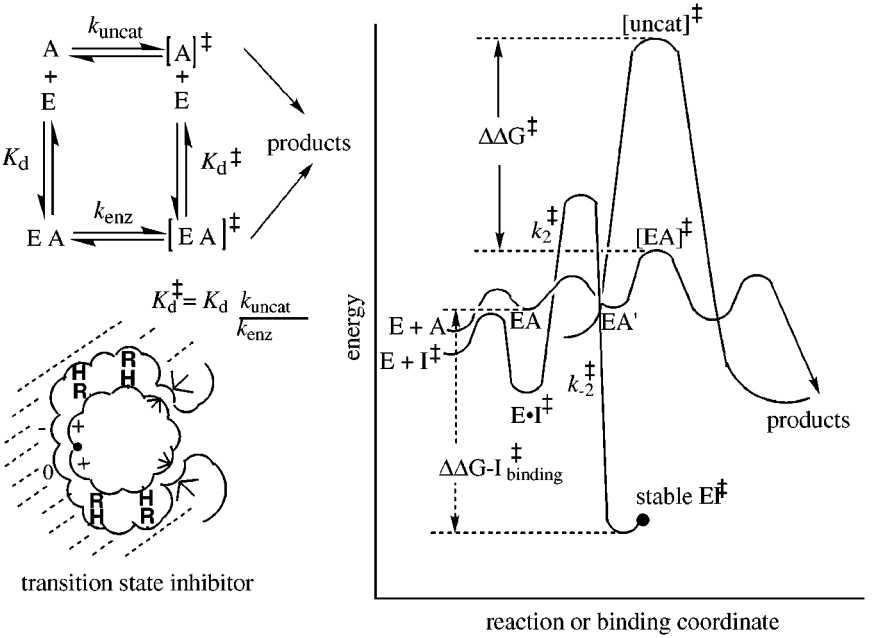

Figure 2 The thermodynamic box that predicts transition state binding affinity (*upper left*) compares the rates of uncatalyzed (k_{uncat}) and enzymatic (k_{enz}) reactions and assumes that the transmission coefficients from $[A]^‡$ and $[EA]^‡$ are equal. The dissociation constants for EA and $[EA]^‡$ are given by K_d and $K_d^‡$. Transition state inhibitors (*lower left*) invoke the unique ionization and conformational structure found exclusively in the transition state (see Figure 1). Catalysis is prevented by a stable bond at the reaction center (represented by the *solid dot*). The energetics of catalysis and binding an energetically perfect transition state analog are compared in the reaction or binding coordinate diagram. Energy of enzymatic transition state stabilization ($\Delta\Delta G^‡$) is converted into binding energy for the transition state inhibitor ($\Delta\Delta G\text{-}I^‡$) to form the stable $EI^‡$ complex, which cannot escape by the product release pathway. The slow-onset inhibition common with transition state inhibitors occurs after formation of a readily reversible $E{\cdot}I^‡$ complex. The rate of onset for tight-binding inhibitors is $k_2^‡$ and the rate of escape is $k_{-2}^‡$. Note the unfavorable energetic barrier for escape from the stable $EI^‡$ complex.

in response to inhibitor development for the AIDS protease, β-lactamases, metalloproteinases, cyclooxygenases, and a growing list of enzymes that are targets for pharmaceutical intervention. Because many inhibitor developments are proprietary, the list for 1995 is likely to be an incomplete representation of the known list of transition state inhibitors.

In 1947, an experimental approach to chemical transition states was discovered by Bigeleisen and coworkers, who, along with others, established the relationships among isotopic substitution, altered reaction rates, and altered bonding between reactants and transition states (8–10). A few applications

of individual kinetic isotope effects were made to enzymatic reaction mechanisms before 1970. Qualitative results from these studies indicated whether the bond changes to the isotopically labeled atom occurred in the rate-limiting step (e.g. Figure 1). The Steenbock Symposium of 1976, "Isotope Effects on Enzyme-Catalyzed Reactions," provided the impetus for additional studies on enzymes (11). The 1978 book *Transition States of Biochemical Processes* included the provocative and fundamentalist position of RL Schowen that "the entire and sole source of catalytic power is the stabilization of the transition state; that reactant-state interactions are by nature inhibitory and only waste catalytic power" (12, p. 78). These works bridged the gap between chemical and biological transition states, recognizing that even complex biological transformations involve formation of one or more defined transition states and are therefore susceptible to transition state analysis based on the measurement of kinetic isotope effects. Development of steady state and pre–steady state kinetic methods to reveal intrinsic isotope effects permitted interpretation of results in terms of transition state structure (13–17).

Although the focus of this review is enzymatic transition states and related inhibitors, transition state similarity is not necessary for tight-binding inhibition of enzymes. Any combination of multiple favorable hydrogen, ionic, or hydrophobic bonds between enzyme and substrate can provide the summation of binding interactions leading to tight-binding inhibition and is the basis for inhibitory screening from chemical and combinatorial libraries. Examples of such inhibitors are found in nature as antibiotics. Streptomycin, erythromycin, and rifampicin are examples of complex natural products that have no known similarity to the transition states involved in protein and RNA synthesis. Inhibitors designed to match contacts in the catalytic site or those that are stable analogs of the substrate can bind tightly but do not qualify as transition state inhibitors. One example is the tight binding of methotrexate to dihydrofolate reductase, in which the analog is bound upside down with respect to substrate in the catalytic site (18). Another example is 9-deaza-9-phenyl-guanine, a powerful inhibitor of purine nucleoside phosphorylase. It was designed from the X-ray crystal structure of substrate and product complexes and does not resemble the transition state (19, 20) (Figure 3).

TRANSITION STATE THEORY FOR ENZYME-CATALYZED REACTIONS

Nature of the Transition State

As substrate progresses from the Michaelis complex to product, chemistry occurs by enzyme-induced changes in electron distribution in the substrate. Enzymes alter the electronic structure by protonation, proton abstraction, electron

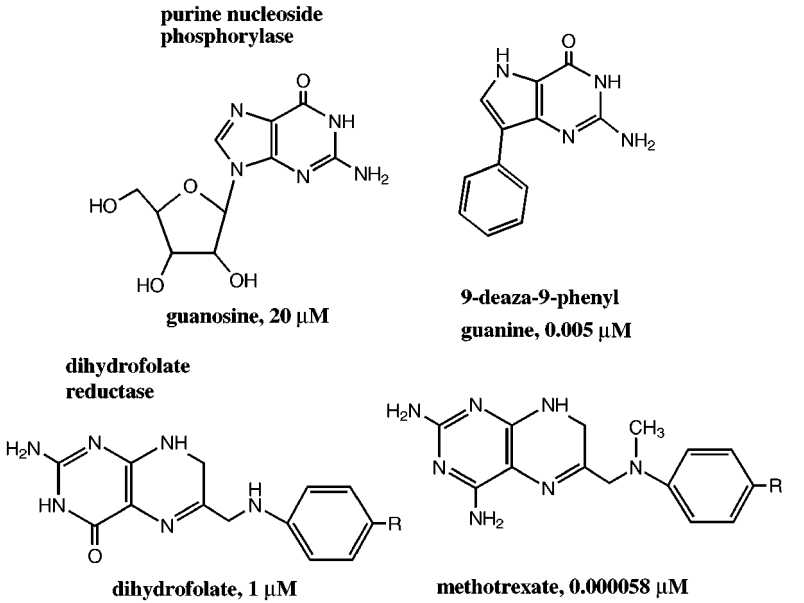

Figure 3 Tight-binding inhibitors of purine nucleoside phosphorylase and dihydrofolate reductase that are not transition state analogs despite high-affinity binding. The K_m values for substrates and equilibrium K_i values for the inhibitors are shown.

transfer, geometric distortion, hydrophobic partitioning, and interaction with Lewis acids and bases. These are accomplished by sequential protein and substrate conformational changes (Figure 1). When a constellation of individually weak forces are brought to bear on the substrate, the summation of the individual energies results in large forces capable of relocating bonding electrons to cause bond-breaking and bond-making. Substrates of modest molecular size (for example, glucose), bound in the active sites of proteins, typically interact with two H-bonds at each donor/acceptor site. These interactions alone, in typical H-bond energies of 3 kcal/mol/H-bond, can provide over 30 kcal/mol of energy toward redistribution of electrons and therefore toward ionizations and covalent bond changes. The restricted geometry and hydrophobic environment allow short H-bonds to form that would be unfavorable in solution (21, 22).

The lifetime for chemical transition states is short, approximately 10^{-13} sec, the time for conversion of a bond vibrational mode to a translational mode (23, 24). This theory requires reexamination for enzymes, because the protein domain motion resulting in transition state formation may stabilize the altered bond lengths of the bound transition state for a lifetime sufficient for 10^1–10^6

vibrations. This hypothesis is indicated by the dimpled transition state feature labeled with a question mark in Figure 1; it remains unexplored except by computational theory. Enzymes that form transient covalent intermediates require two distinct transition states. These transition states are surrounded by lower energy complexes and should be distinguished from the altered vibrational state implied by the question mark in Figure 1. The classic interpretation of the transition state supposes a short lifetime during which an infinitesimal force toward product or substrate leads to EP′ and EA′ respectively.

Induced Protein Conformational Change

The energetic problem that must be solved by enzymes is to bind tightly only to the unstable transition state structure while avoiding tight binding to the substrate and products. Enzymes often bind to the substrate at diffusion-controlled rates, and subsequent conformational or electronic changes are mandatory for catalysis. Placing the enzyme-bound substrate in the solvent-restricted environment of the closed catalytic site permits the subsequent events to occur in the altered solvent of the catalytic site.

Presenting the enzyme with a transition state mimic results in a mismatch of the substrate-recognizing features. Many transition state inhibitors are slow-onset, typified by a rapid weak binding followed by a slow tight-binding interaction. The energetics of this interaction (Figure 2) show rapid formation of the encounter complex E·$I^{‡}$ (similar to the EA complex of Figure 1) followed by a difficult (high-energy, slow) entry to the stable $EI^{‡}$ complex. The bound inhibitor does not induce the conformational change with the efficiency of substrate and requires time to permit the transition state conformational change to occur on the protein. This time corresponds to the slow onset of tight-binding inhibition commonly observed with transition state mimics (6). These data argue that the substrate actively induces the catalytic conformational change, because the rate of catalysis is substantially greater than the rate at which most tight-binding inhibitors induce enzymes into the transition state configuration. This view of transition state inhibitor interaction predicts that near-perfect inhibitors would still exhibit slow-onset inhibition because the enzyme is designed to recognize the ground state of the substrate. However, some tightly bound inhibitors are reported to achieve inhibition on the time scale of catalysis. For example, the inhibition of adenosine deaminases by purine riboside and of cytidine deaminase by pyrimidin-2-one riboside is fast (25–26). These inhibitors are estimated to bind with dissociation constants of 10^{-13} and 10^{-12} M respectively, approaching the hypothetical 10^{-16} M dissociation constant for the actual transition states. Rapid onset occurs because these are half-reaction substrates for the enzymes. The deaminases contain a tightly bound zinc that acts as the catalytic site base to ionize a water molecule to the hydroxide and position it near

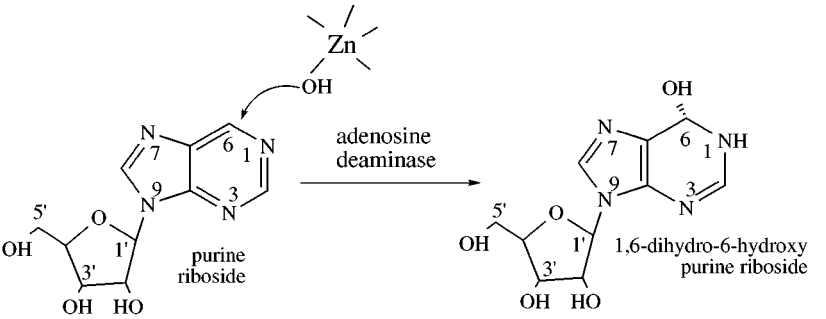

Figure 4 Hydration of purine riboside by a catalytic site hydroxyl generated at the tightly bound Zn^{2+}. The hydrated purine is bound tightly. An analogous reaction occurs with cytidine deaminase.

the reactive carbon of the aromatic rings (27; Figure 4). Enzymatic protonation of the adjacent aromatic ring nitrogen assists in the required rehybridization of the rings. These inhibitors take advantage of the substrate-induced transition state configuration to cause rapid hydration and tight binding of the hydrated species. The sp^3 hybridization at the reactive carbon is a transition state feature, and without the amino leaving group, a stable complex is formed.

Tight Binding of the Transition State Structure

Binding energies of enzymatic transition states are generated by the realignment of substrate (Michaelis) contacts as the enzyme and substrate mutually change their structures toward the transition state (Figure 1). The strong dependence of hydrogen and ionic bond energy on bond distance, angle, solvent environment, and relative pK_a values can be invoked to explain the increases in binding forces of the transition state complex relative to the Michaelis complex (21, 28). Structural rearrangements tighten the protein around the catalytic site to exclude solvent and to make stronger electrostatic contacts. These are shown as well-aligned H-bonds at the transition state and as ionic attraction and repulsion as catalytic forces (Figure 1). Enzymatic reactions usually demonstrate distinct pK_a values for substrate binding and k_{cat}, testifying to the ionic changes between the enzyme substrate and enzyme transition state complexes (29, 30). A common mechanism for enzymatic catalysis is to generate differential charge between substrate and transition state, permitting electrostatic interactions to specifically stabilize the transition state (28). The imperfect match between the enzyme and the transition state inhibitor is inevitable because it is impossible to recreate perfectly the nonequilibrium bond lengths of the transition state with stable compounds. The $\Delta\Delta G\text{-}I^{\ddagger}_{binding}$ energy of Figure 2 is shown for a perfect transition state inhibitor, with full $K_d^{\ddagger}$ of the transition state. For the necessarily

imperfect transition state inhibitors, the $k_2^{\ddagger}$ barrier is the time to fit the imperfect inhibitor into the lowest-energy structure of the analog complex.

Relaxation of the Transition State Complex

Catalysis requires rapid relaxation of the transition state energy to allow the products to dissociate. The relative enzymatic affinity for the transition state and products decreases by about 12 orders of magnitude within milliseconds. For catalytically efficient enzymes, the Michaelis complex is a diffusional event with a rate constant near 10^9 $M^{-1}sec^{-1}$. Transition state formation, product formation, and release are as rapid as this, so the diffusional event defines the maximal catalytic rate (31). The change in electron distribution as bonds are broken creates a repulsive interaction that opens the catalytic site and expels products (see Figure 1). This step is the opposite of what occurs when the Michaelis complex is converted into the transition state complex.

Computer modeling of well-understood enzymatic reactions has allowed examination of the factors important in catalysis. The resulting conclusion is that electrostatic stabilization of the transition state is the most significant factor (28). Understanding the electrostatic nature of the transition state therefore provides a template for the synthesis of transition state inhibitors. The experimental approach that provides the most direct information for enzymatic transition state structure is analysis of kinetic isotope effects (32–34).

EXPERIMENTAL APPROACHES TO ENZYMATIC TRANSITION STATE STRUCTURE

Chemical Precedent

Chemical reactivity series with leaving groups of different pK_a values or electron withdrawing capability can indicate the position of the transition state in the reaction coordinate. Brønstead and Hammett plots have had wide application in chemical mechanisms, but less in enzymology because the specificity of enzymes often does not permit the use of a variety of substrates (35, 36). Behavior of model chemistry in solution for the reaction of interest provides a transition state benchmark for comparison with the transition state structure imposed by the enzyme.

Transition State Inhibitors

Inhibitors that bind tightly, are slow-onset, and resemble the expected transition states have been used to predict state features (4–6). For example, the inhibition of deaminases and proteases by analogs with sp^3 reaction centers was useful in establishing the nature of these transition states and intermediates (37, 38). Inhibitor specificity is subject to the vagaries of enzymatic binding

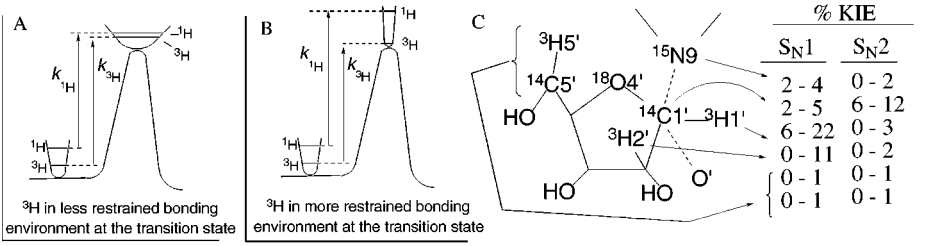

Figure 5 Simplified bond vibrational basis for the relationship between a kinetic isotope effect and transition state structure. The parabolae represent the bonding environment (restoring force) for the vibrational mode of a bonded atom (^{1}H) and its isotope (^{3}H) in the reactant and transition states. The *arrows* are the activation energies for ^{1}H- and ^{3}H-labeled reactants. In *panel A*, ^{1}H-substrate reacts more rapidly (has lower activation barrier). In *panel B*, ^{3}H-substrate reacts more rapidly (has lower activation barrier). In practice, all significant modes are considered. In *panel C* are the anticipated values of kinetic isotope effects for C1′-N9 N-ribosidic bond scission with S_N1 or S_N2 character. The ranges arise from variability in ring geometry and the degree of the associated O′ nucleophile at transition states with predominant S_N1 or S_N2 character. The percent kinetic isotope effect (%KIE) = [(unlabeled rate/labeled rate) − 1.00] × 100%.

sites. Transition state properties cannot always be predicted, as demonstrated by methotrexate in the catalytic site of dihydrofolate reductase (18; Figure 3). Direct information on transition state structure is available from kinetic isotope effect studies.

Kinetic Isotope Effects

The only method available for the direct determination of enzymatic transition state structure is the measurement of kinetic isotope effects. Excellent accounts of the theory and its development can be found in the literature (39–43) and are beyond the scope of this review. Kinetic isotope effects compare the enzymatic reaction rates of isotopically labeled and unlabeled substrates (Figure 5). Isotopically labeled molecules have molecular energy different from that of unlabeled molecules and thus require a different amount of energy to reach the transition state, where the molecular energies may also be perturbed by the isotope. If the bonding environment for the labeled atom is less restricted in the transition state than in the reactant, the isotope effect will be normal (the heavy isotope substrate reacting more slowly than the unlabeled substrate). Likewise, if the bonding environment at the transition state is more restricted than for the reactant, the substrate with the higher mass isotope will react more rapidly (an inverse kinetic isotope effect). Isotope effects also provide quantitative information because the magnitude of the isotope effect indicates the extent of bond change. For some isotope effects, bond geometry can be determined because of

the dihedral angular dependence for conjugative isotope effects β to the bond being broken (44, 45). By measuring kinetic isotope effects at every position in a substrate molecule that might be expected to be perturbed at the transition state, a unique description of the transition state can be deduced if intrinsic isotope effects are being measured (13, 46). The steps involved in transition state analysis by kinetic isotope effects are to

1. synthesize substrates with appropriate isotopic labels
2. measure kinetic isotope effects to an accuracy of better than 0.5%
3. compute a truncated transition state with bond lengths and angles matching the isotope effects (limited to 25 atoms), using normal-mode bond-energy bond-order vibrational analysis (47, 48)
4. restore the complete molecular structure for the transition state by fixing the bonds established from kinetic isotope effects and optimizing the remaining structure using semiempirical methods (49)
5. determine the electron wave function for the molecule to determine electron distribution at the van der Waals surface (50).

EXAMPLES OF ENZYMATIC TRANSITION STATES

AMP Nucleosidase

AMP nucleosidase catalyzes the hydrolysis of AMP to adenine and ribose 5-phosphate under the allosteric control of MgATP and inorganic phosphate, which serve as allosteric activator and inhibitor, respectively (51, 52):

$$\text{AMP} + \text{H}_2\text{O} \rightarrow \text{adenine} + \text{ribose 5-phosphate}.$$

The enzyme is found only in prokaryotes and is thought to play a role in the regulation of energy metabolism. However, genetic ablation of the enzyme from *Escherichia coli* had only minor effects on growth rates (53). The enzyme from *Azotobacter vinelandii* requires MgATP as a k_{cat} activator. In the absence of activator, the enzyme binds substrate, but k_{cat} is 10^{-3} of that with the allosteric activator. This provides the opportunity to determine whether allosteric activation is capable of changing the chemical nature of the transition state or only serves to change energies of activation (altered rate constants) for steps through the reaction cycle. Systematic determination of kinetic isotope effects is made possible by the combined chemical and enzymatic synthesis of AMP (Figure 6) with the isotopic labels indicated in Figure 7 (54–56).

Kinetic isotope effects for the enzyme were intrinsic based on the catalytic mechanism and by comparison with the isotope effects for acid-catalyzed

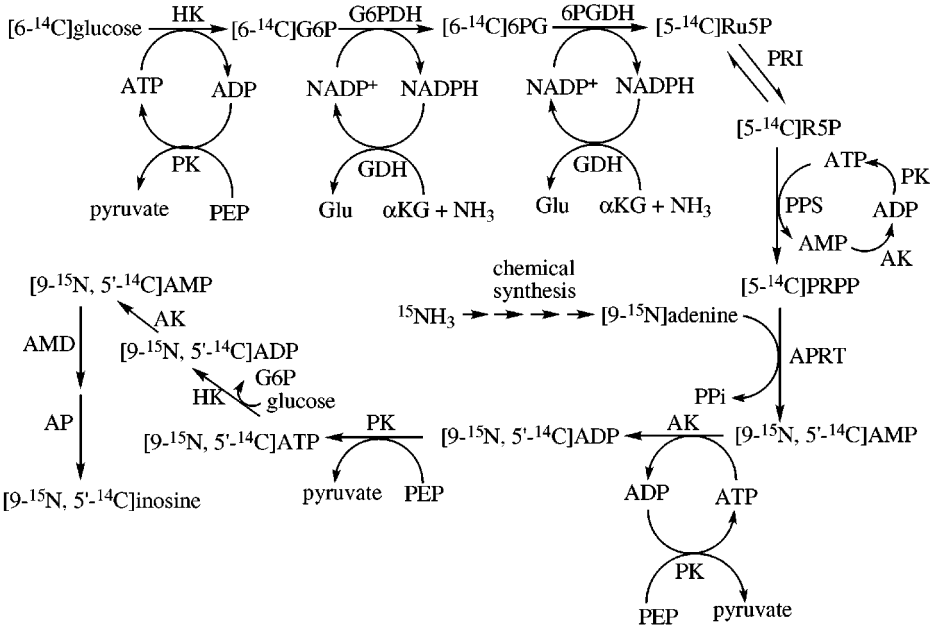

Figure 6 Combined enzymatic and chemical synthesis of specifically labeled nucleosides and nucleotides (synthesis of [9-^{15}N, 5′-^{14}C]ATP, AMP, and inosine). All steps from glucose to ATP are coupled in a single reaction mixture. Separate reaction mixtures are used to convert ATP to AMP and to inosine. The enzymes are HK = hexokinase, PK = pyruvate kinase, G6PDH = glucose 6-phosphate dehydrogenase, 6PGDH = 6-phosphogluconate dehydrogenase, GDH = glutamate dehydrogenase, PRI = phosphoriboisomerase, PPS = 5-phosphoribosyl-1-pyrophosphate synthetase, AK = adenylate kinase, APRT = adenine phosphoribosyltransferase, AMD = AMP deaminase, AP = alkaline phosphatase. Using specific labels in glucose, ribose and adenine can yield the desired labels at any position of the nucleosides and nucleotides.

solvolysis of AMP (56). The transition state for the acid-catalyzed reaction was compared to those determined for the enzyme in the presence and absence of allosteric activator (Figure 7). Because kinetic isotope effects report directly on the bond environment at the transition state, comparison of the experimental kinetic isotope effects established that the transition states differ for the enzyme-catalyzed and acid-catalyzed hydrolysis. The allosteric activator, which causes a 10^3-fold increase in catalytic rate, also changes the nature of the transition state. Quantitiation of the isotope effects in terms of bond orders for reactants and transition states indicated that the enzymatic catalyst permitted the reaction to reach the transition state earlier, when there was more bond order remaining

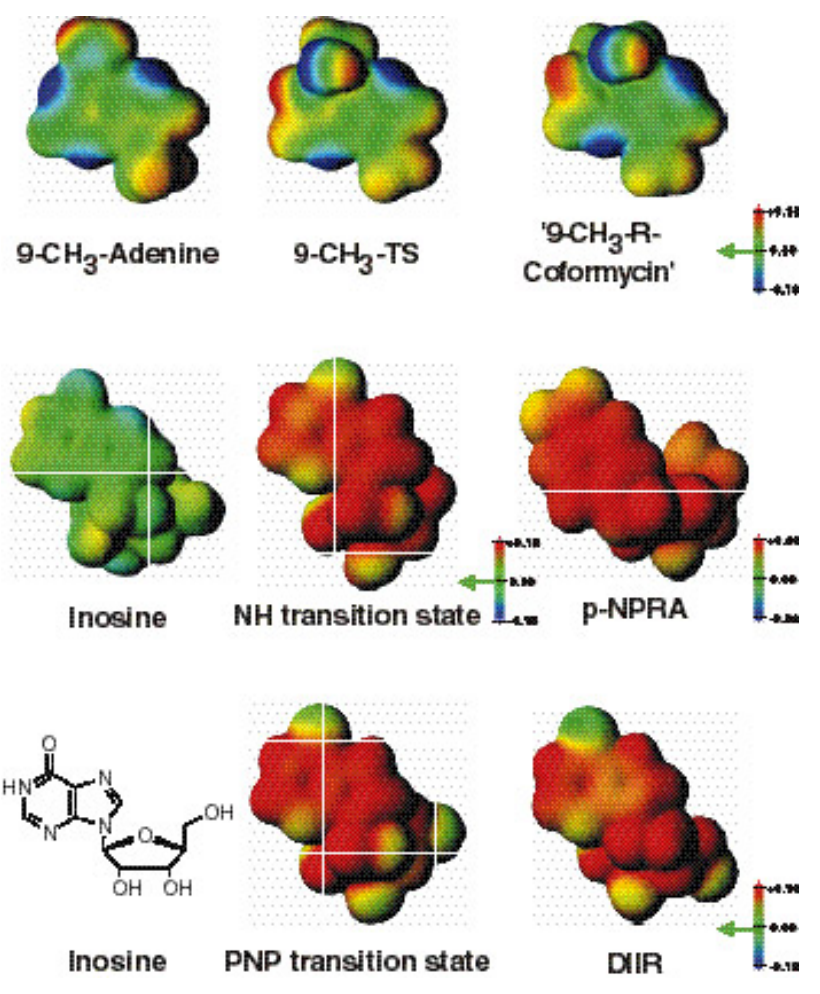

Figure 10 Molecular electrostatic potential at the van der Waals surfaces for substrates, transition state, and transition state inhibitors for AMP deaminase (*top*), nucleoside hydrolase (NH) (*center*), and purine nucleoside phosphorylase (PNP) (*bottom*). The chemical structure of inosine is shown. Other structures are shown in Figures 9, 11, and 12. Details of the calculations are in References 82, 89, and 92. In every case, the electrostatic potential similarity between the transition state and the transition state inhibitor is greater than between the substrate and the transition state. The attacking water and phosphate nucleophiles are omitted from the transition state structures for NH and PNP. The color codes for the molecular electrostatic potentials are shown to the *right*.

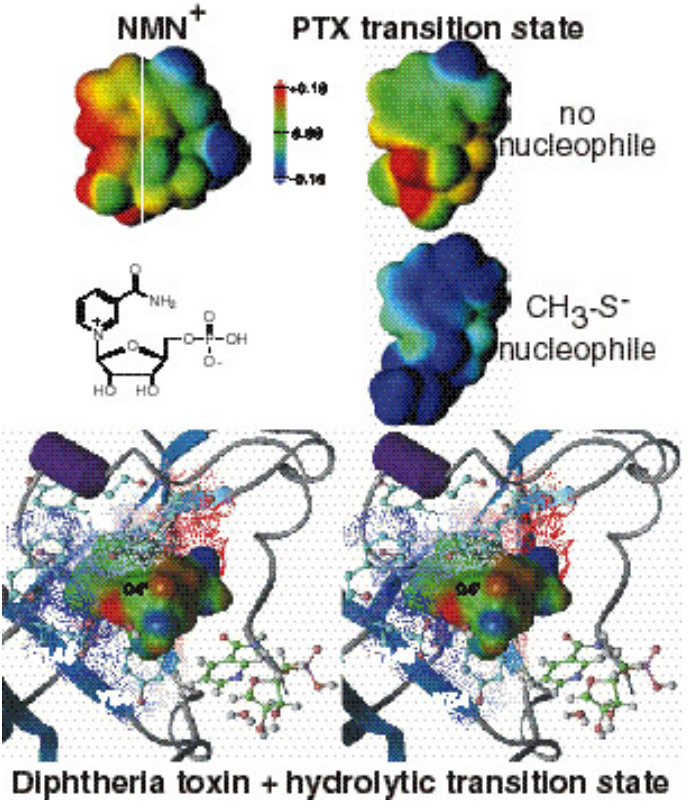

Figure 17 Electrostatic potential surfaces for NMN^+, the transition state for NAD^+ hydrolysis by pertussis toxin (PTX) showing only the NMN^+ portion, and the transition state for ADP-ribosylation of the C-terminal 20–amino acid peptide from $G_{i\alpha 3}$ by pertussis toxin showing only the atoms of NMN^+ and a CH_3S^- to replace the peptide. A docked model of the transition state for diphtheria toxin in the crystal structure of diphtheria toxin is shown in stereo. The chemical and electrostatic potential surface for NMN^+ is shown in the *upper left*. At the transition state, the nicotinamide positive charge migrates into the ribosyl, forming the ribooxocarbenium. In the no-nucleophile structure, the charge (*red*) is clearly visible. Participation of the thiolate anion at the transition state causes the charge gradient to be lost across the susceptible bond, so that both the nicotinamide and ribosyl are partial negative (*blue*), causing C1-N1' bond scission with lagging attack of the thiolate anion (CH_3S^-). Docking the no-nucleophile transition state into the crystal structure for diphtheria toxin shows electrostatic complementarity, especially at E148, the essential catalytic site carboxylate that interacts with the positive charge (*red*) of the oxocarbenium ion. The stick model to the *lower right* of the stereo figure shows NMN^+ and the attacking water nucleophile in the same relative orientation of the transition state embedded into the protein.

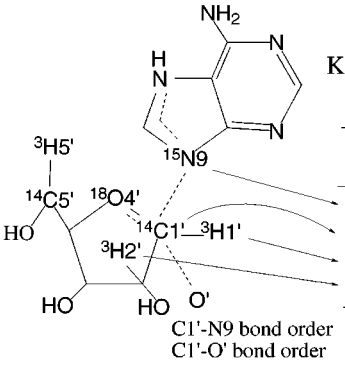

Kinetic Isotope Effects for AMP Nucleosidases

	% KIE				
		native		mutant	
	acid	-MgATP	+MgATP	-MgATP	+MgATP
	3.0	3.0	2.5	3.4	2.1
	4.4	3.5	3.2	4.1	4.1
	21.6	6.9	4.7	8.6	9.4
	7.7	6.1	4.3	8.9	8.6
C1'-N9 bond order	0.02	0.16	0.21	0.09	0.18
C1'-O' bond order	0.02	0.03	0.03	0.03	0.01

Figure 7 Kinetic isotope effects (KIEs) and bond orders at the transition states for the C1′-N9 bond hydrolysis of AMP by acid and AMP nucleosidases. All isotope effects were measured with a mixture of two AMP molecules, one labeled near and one distant from the C′1-N9 bond. Both native and mutant enzymes were activated by a factor of $\sim 10^3$ by the addition of MgATP. Kinetic isotope effects were measured with average standard deviations of 0.4%. Bond orders for the C1′-N9 and C1′-O′ bonds were determined from bond vibrational analysis (48, 56). When bonds surrounding C1′ are weakest at the transition state, the ^{3}H1′ kinetic isotope effect is greatest. Bond order (n) is based on the Pauling rule: $r_n = r_1 - 0.3 \ln n$, where r_1 is the single bond length (58).

to the leaving group (Figure 7). The protein structural change induced by the allosteric activator caused the transition state to occur even earlier in the reaction coordinate. Changes in the transition state structure also resulted from the forced evolution of a β-galactosidase in *E. coli*, causing the enzyme to become catalytically more efficient (57).

Substrate and inhibitor specificity studies revealed that formycin A 5′-phosphate binds $>10^3$ times tighter to AMP nucleosidases than does substrate (59, 60). The X-ray crystal structure of this inhibitor helped to establish the properties of the transition state (61). The inhibitor has a *syn*-ribosyl torsion angle, preferred in all nucleotide inhibitors of the enzyme (59). The molecular electrostatic potential at the van der Waals surface revealed similar electronic structures of inhibitor and transition state because of the common protonation at N7, which is not present in the substrate (62).

Random mutagenesis of the organism expressing AMP nucleosidase provided an enzyme with a k_{cat} 2% that of the native enzyme (Figure 7) (63). The purpose of the mutagenesis was to determine if catalytic site mutation changes transition state structure. The results established substantially different kinetic isotope effects for the mutant enzyme, demonstrating differences in bond structure at the transition state. The mutant enzyme was less effective in stabilizing

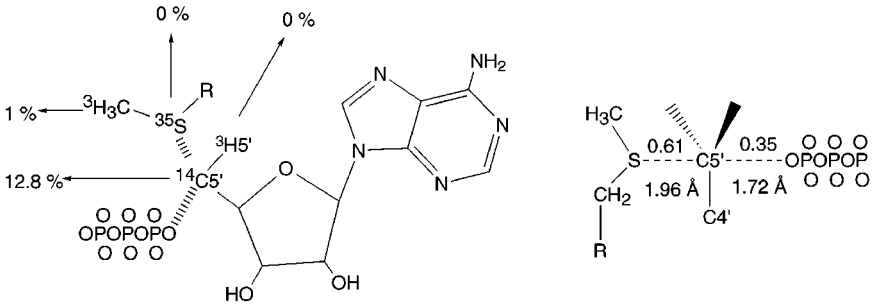

Figure 8 Kinetic isotope effects for the SAM-synthetase reaction (*left*), where the ^{35}S-molecule represents the attacking methionine sulfur nucleophile. The isotope effects were measured in individually labeled substrates but are illustrated here as a single molecule. Only symmetrical S_N2 displacements give primary ^{14}C isotope effects of 12.8% (see Figure 5). The transition state structure consistent with all isotope effects is shown on the *right*. The bond orders were 0.61 and 0.35, which correspond to bond lengths of 1.96 and 1.72 Å for S-C5′ and C5′-O bonds, respectively. The mass difference between sulfur and oxygen accounts for the differences, which are equivalent in bond vibrational energy. C5′ is the center of reaction coordinate motion, giving the large ^{14}C isotope effect.

the ribooxocarbenium ion of the transition state and in protonating the adenine leaving group (64).

S-Adenosylmethionine Synthetase

The chemical reaction of S-adenosylmethionine (SAM) synthetase involves displacement of the tripolyphosphate of ATP by reaction of the sulfur of methionine with C5′ of ATP (Figure 8). The reaction results in the further hydrolysis of the phosphate chain to phosphate and pyrophosphate, to release the products SAM, phosphate, and pyrophosphate from the catalytic site (65–66). This is one of the few reactions of ATP in which all phosphates are displaced in a single reaction. The reaction is irreversible under physiological conditions as a consequence of the tripolyphosphorolysis. Potassium ion is required for efficient catalysis, activating the enzyme approximately 100-fold. Kinetic isotope effect studies of the enzyme were designed to establish the nature of the transition state under optimal catalytic conditions and to establish the effect of K^+ ion activation. Monovalent cations are common in kinase activation and are thought to provide a positive charge to neutralize the transition state complex at highly charged reaction centers typified by phosphoryl transfers (67). Activation can be achieved either by changing a rate constant or by changing the transition state structure.

Measurement of kinetic isotope effects with limiting K^+ gave intrinsic isotope effects (68). The ^{14}C5′ kinetic isotope effect was 12.8%, near the theoretical

limit for a primary ^{14}C isotope effect (33). This value is realized only when carbon dominates reaction coordinate motion in a symmetric nucleophilic displacement reaction. The result provided a ready solution for the reaction mechanism. In nucleophilic displacements, neighboring α- and β-secondary ^{3}H isotope effects are expected to be insignificant, and this was confirmed for both [5′-^{3}H]ATP and methyl-[$^{3}H_3$]methionine. These kinetic isotope effects provide proof that the chemical mechanism of SAM synthetase at limiting K^+ is a symmetric S_N2 reaction. Addition of K^+ to activate the rate by 100-fold decreased the [5′-^{14}C]ATP isotope effect, consistent with either a change in transition state structure or increased forward commitment (Figure 1).

Substrate trapping experiments, pioneered by I Rose (69), permitted the direct measurement of forward commitment for SAM synthetase (the probability that a bound substrate molecule will be transformed to product relative to release from the catalytic site). Only substrate molecules in equilibrium with free substrate contribute to the observed isotope effect (13). The results established that K^+ improved catalytic efficiency by increasing the forward commitment. The intrinsic isotope effect (corrected for commitment) was unchanged, thus the structure of the transition state is unchanged by K^+. This example of enzymatic activation demonstrates lowering the transition state energetic barrier without a measurable change in the bond environment of the transition state (Figure 1).

AMP Deaminase and Adenosine Deaminase

The deaminations of AMP and adenosine are aromatic nucleophilic substitutions at carbon, a reaction type well known in chemistry and characterized by rate-limiting formation of an unstable tetrahedral intermediate that decomposes rapidly to yield products (70). AMP deaminase is found only in eukaryotes, and it is proposed to be involved in the regulation of the adenine nucleotide pool through the purine nucleotide cycle (71). Activation of AMP deaminase in times of energy deficiency leads to IMP formation and a decrease in the total adenylate pool size (72). Humans deficient in specific muscle isozymes of AMP deaminase suffer moderate difficulty in muscular work, but deficiencies in the erythrocyte/heart isoform have no known phenotype (73). It has been proposed that inhibition of the heart isozyme during recovery from heart attacks might speed recovery by preserving the adenylates and preventing oxygen radical damage associated with the conversion of hypoxanthine to uric acid (74). Adenosine deaminase deficiency leads to B- and T-cell immunodeficiency, presumably as a result of the accumulation of dATP in the progenitor cells preventing clonal expansion in response to an immune challenge (75).

The natural products coformycin, deoxycoformycin, and their 5′-phosphates are tight-binding transition state inhibitors for adenosine and AMP deaminases, binding approximately 10^7-fold more tightly than substrates (76–78). The

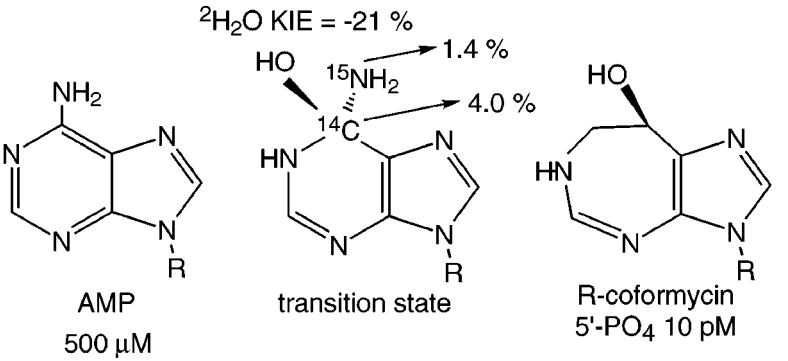

Figure 9 Substrate, transition state, and transition state inhibitor for yeast AMP deaminase. The kinetic isotope effects (KIEs) are superimposed on a diagram of the transition state. The R-substituent is ribose 5′-phosphate. The isotope effects were measured using the natural abundance of ^{15}N, specifically labeled ^{14}C-AMP, and with solvent deuterium for the ^2H_2O KIE.

transition state structures of these enzymes are of interest for comparing transition state structure deduced from kinetic isotope effects to the structures of transition state inhibitors. Specific questions about the nature of the transition states include the degree of hydroxyl attack (sp^3 hybridization) at C6 in the transition states; whether protonation of the leaving amino group has occurred; whether amino group departure has begun; and whether the enzymatic transition state structures can explain the tight binding of the coformycins.

Kinetic isotope effects from yeast AMP deaminase were similar to those measured for adenosine deaminase, indicating that both have similar transition states (Figure 9; 79, 80). The conserved protein motif for the catalytic site zinc also supports common catalytic site chemistry (81). The enzyme-stabilized transition state is reached prior to formation of the tetrahedral intermediate, at a bond order of 0.8 to the incoming water nucleophile, while retaining full bond order to the leaving amino group. The increased bond order to the attacking water oxygen requires that the purine ring lose its conjugation and that N1 become protonated to reach the transition state. Before the N6 amino group is competent for departure, it must be protonated, a process that occurs in a rapid step after transition state formation. The transition state is early, preceding formation of the intermediate. Formation of the intermediate, protonation, and loss of the exocyclic amino group are all fast relative to the initial addition of water to form the transition state.

Molecular electrostatic potential surface analysis of the transition state and substrate reveals substantial changes and compelling similarity between the transition state and coformycin (Figure 10, color plate) (82). The striking

correspondence indicates that the molecular electrostatic potential surface of this transition state is closely related to that for the transition state inhibitor.

Nucleoside Hydrolase

Protozoan parasites are purine auxotrophs, using salvage enzymes to recover purines from their environment (83). The nucleoside hydrolases cleave the N-ribosidic bonds of nucleosides to liberate the purine and pyrimidine bases and to generate ribose (84–88):

$$\text{nucleosides} + H_2O \rightarrow \text{base} + \text{ribose}.$$

Liberated bases are salvaged by phosphoribosyltransferases. Ribosyl nucleoside substrates and substrate analogs bind poorly to the nonspecific nucleoside hydrolase from *Crithidia fasciculata* with dissociation constants from 0.2 to 10 mM (84). The nucleoside hydrolases are not found in mammalian genomes; thus the enzymes have been targeted for antiprotozoan agents (89, 90). A goal of this study was to characterize the transition state for the nonspecific nucleoside hydrolase from *C. fasciculata* and use the information to design transition state inhibitors. At the transition state, the N9-C1′ ribosidic bond cleavage is well advanced, with 0.22 bond order remaining (Figure 11). The attacking water

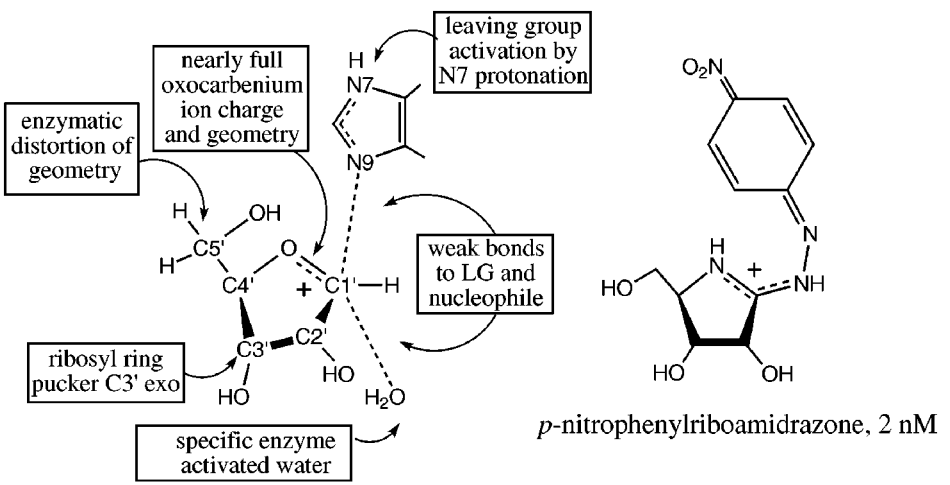

Figure 11 Features of the transition state for the nonspecific nucleoside hydrolase from *Crithidia fasciculata*. The substrates were labeled inosines (Figure 12) synthesized as in Figure 6, and the isotope effects were interpreted according to normal-mode and ab initio methods (89, 90). A tight-binding transition state inhibitor is shown on the *right*. The resonance structure of the inhibitor bound to the enzyme was determined by resonance Raman spectroscopy.

nucleophile lags well behind N-ribosidic bond breaking with approximately 0.03 bond order from the attacking oxygen to C1′. The loss of most of the N-ribosidic bond before water attacks leaves the ribose as an oxocarbenium cation at the transition state with C1′ rehybridized nearly completely to sp^2. This flattens the ribose ring around C1′, causing the atoms of the ribosyl ring to be coplanar with the exception of C3′. The kinetic isotope effect from ^{3}H2′ is dependent on the dihedral angle to the C1′-N9 bond. Its value required that C3′ lies below the plane of the ring, in the C3′-*exo* ribosyl configuration, to provide near eclipse in the H2′-C2′-C1′-N9 dihedral angle. Solvent D_2O and ^{15}N9 isotope effects established that the hypoxanthine leaving group is protonated, most likely at N7, prior to reaching the transition state. This creates a neutral, planar, and hydrophobic leaving group. A suprising remote 5′-^{3}H isotope effect of 5.1% was observed in the enzyme but not in acid-catalyzed hydrolysis of inosine, establishing enzyme-induced distortion (89, 90). The interpretation that the 5′-oxygen is rotated above the oxocarbenium ion is shown in Figure 11 and was recently confirmed by X-ray crystallogaphic studies with a bound transition state inhibitor (90a).

Based on the transition state structure, iminoribitol and riboamidrazone inhibitors with K_m/K_i to 200,000 have been synthesized and characterized (90–94). The best inhibitor (*p*-nitrophenylriboamidrazone; Figure 11) incorporates most of the electrostatic traits of the transition state but is structurally distinct from both the substrate and transition states. The similarity to the transition state is apparent in the comparison of the molecular electrostatic potentials of substrate, transition state, and transition state inhibitor in Figure 10 (color plate) (95). Thus, the molecular electrostatic potential surface matching of inhibitor and transition states leads to powerful binding energy.

Purine Nucleoside Phosphorylase

Scission of the N-ribosidic bonds of the purine nucleosides and deoxynucleosides in mammals is accomplished almost exclusively by the phosphorolysis reaction of purine nucleoside phosphorylase (PNP). Inosine, guanosine, and 2′-deoxyguanosine are the major substrates. The genetic deficiency of human PNP causes a T-cell deficiency as the major physiological defect (96). Apoptosis in T cells that are not immunologically stimulated to divide results in recycling of DNA in these thymic cells. When PNP is absent, 2′-deoxyguanosine is converted to dGTP instead of being degraded. Imbalance of deoxynucleotides prevents clonal expansion of normal T-cell populations. Several human disorders may involve T-cell action, including T-cell lymphoma, lupus, psoriasis, rheumatoid arthritis, and transplant tissue rejection. Specific inhibitors for PNP may provide useful agents for these disorders. The transition state structure of

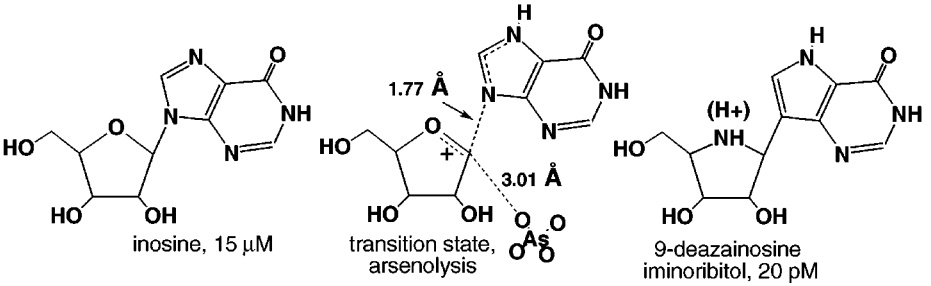

Figure 12 Substrate, transition state, and transition state inhibitor for purine nucleoside phosphorylase. At the transition state, N7 is protonated and the ribosyl is positively charged. These features are incorporated into the transition state inhibitor.

PNP has been determined to permit the development of inhibitors related to the transition state.

Transition state analysis was accomplished using arsenate (AsO_4) because in the presence of phosphate, commitment factors prevented measurement of intrinsic isotope effects (20). In the absence of phosphate or arsenate, the enzyme catalyzes the slow hydrolysis of inosine at one of the trimeric catalytic sites but retains tightly bound hypoxanthine (97). Under these conditions, pre–steady state isotope effects were intrinsic and permitted the hydrolytic and arsenolysis transition states to be compared (98). A fundamental question for the transition state of PNP is the degree to which the transition state is nucleophilic (extent of arsenate or phosphate bonding to C1′ at the transition state), because the reaction occurs with inversion of configuration, as expected for nucleophilic displacements. The results shown in Figure 12 establish that the transition state for arsenolysis is oxocarbenium ion in character, with bond order 0.4 to the leaving group but bond order <0.04 to the incoming water or arsenate oxygens. The enzyme forms an enzyme-bound ribooxocarbenium ion without bound phosphate or arsenate, and participation of the attacking nucleophile occurs late in the reaction coordinate. Formation of the ribooxocarbenium ion requires activation of the purine leaving group, and isotope effects indicate that N7 is protonated at the transition state. The ribose ring accumulates positive charge at the transition state. A transition state inhibitor was designed with a H-bond acceptor at N7 of the purine ring analog, and a positive charge to mimic the ribooxocarbenium ion in the ribosyl analog. 9-Deazainosine iminoribitol is a tight-binding inhibitor binding 10^6-fold tighter than substrate (R Miles, PC Tyler, RH Furneaux, VL Schramm, unpublished data; Figure 12). The molecular electrostatic potential surfaces are compared in Figure 10 (color plate).

Orotate Phosphoribosyl Transferase

Phosphoribosyl transferases were investigated in the pioneering kinetic isotope effects measured by Goiten et al in 1978 (99). The measurement of kinetic isotope effects from both [1-^{3}H]- and [1-^{14}C]5-phosphoribosyl-1-pyrophosphate suggested a pattern consistent with a dissociative mechanism, with pyrophosphate departure being well developed prior to the attack of the nitrogen from the purine. However, many of the phosphoribosyl transferases demonstrated substantial commitment factors, causing the kinetic isotope effects to be obscured.

Orotate phosphoribosyl transferase (OPRT), similar to other enzymes in this group, does not give useful kinetic isotope effects under normal assay conditions. However, the use of phosphonoacetic acid as a pyrophosphate analog made it possible to study the conversion of orotidine 5′-phosphate to orotate and 5-phosphoribosyl-1-phosphonoacetic acid under conditions that gave intrinsic kinetic isotope effects (100). In reactions with a concerted chemical step, the transition state structure can be determined from kinetic isotope effect measurements in either the forward or reverse directions because the same transition state defines both reactions. Differing chemical reactivity with slow substrates may result in a transition state that differs from the normal reaction. However, these differences are expected to be small because the template of the catalytic site is expected to favor a specific transition state geometry for the reaction.

At the transition state for OPRT, the N1-C1′ bond has a residual bond order of 0.28 and the attacking oxygen from the pyrophosphate analog is just beginning to participate with a bond order of <0.02 (Figure 13). The kinetic isotope effect from [2′-^{3}H]orotidine 5′-phosphate is relatively large at 14%, establishing that the dihedral angle to the leaving group is nearly eclipsed. The remote 5′-^{3}H isotope effect is significant at 2.8%, confirming that ribosyl-transferases commonly use geometric distortion from the ribosyl 5′-position to form the transition state geometry. Features of this transition state require a ribooxocarbenium ion structure. The X-ray crystal structure of the enzyme has been solved with orotidine 5′-monophosphate or 5-phosphoribosyl-1-pyrophosphate at the catalytic site (101, 102). Although the structure is not in a transition state conformation, Arg156 is shown to interact with the 4-carbonyl group of orotic acid and can be proposed to activate the orotic acid leaving group.

NAD^{+} and the ADP-Ribosylating Toxins: Cholera, Diphtheria, and Pertussis

Early investigations of the hydrolysis of nicotinamide from NAD^{+} and NMN^{+} in solution and by NAD^{+} hydrolases used [1′-^{2}H]- in NAD^{+} or NMN^{+} as the isotopic probes (103–104). Based on the cases where isotope effects were observed, the transition states were characterized as dissociative and electropositive.

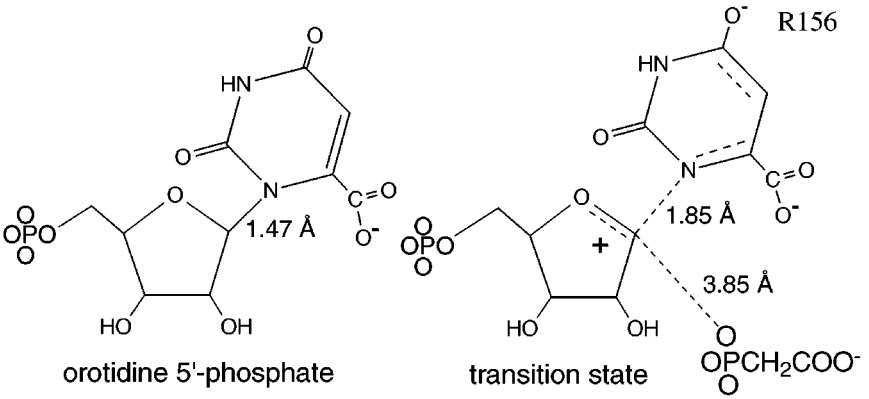

Figure 13 Substrate and transition state for orotidine phosphoribosyl transferase (OPRT) based on kinetic isotope effects. Arg156 appears to be the primary group for stabilizing the leaving group based on the crystal structure. The major enzymatic contacts to the ribosyl are to the 5′-phosphate. Leaving group activation is therefore implicated in forming the transition state from bound orotidine 5′-phosphate.

Recent studies have fully characterized the transition states for NAD^+ hydrolysis in solution and by cholera, diphtheria, and pertussis toxins. These studies have been made possible only by the development of enzymatic synthetic methods to provide specifically labeled NAD^+ (105; Figure 14).

The physiological reaction catalyzed by these bacterial toxins is covalent ADP-ribosylation of regulatory GTP-binding proteins. The covalent modification disrupts the normal functions (106; Figure 15). Because the toxins are a primary cause of tissue damage from these bacterial infections, understanding the transition state structures is intended to guide the design of transition state inhibitors to intervene at the site of tissue damage. An advantage of toxin intervention is that it would not be expected to lead to genetic selection for resistant strains and could be used to limit tissue damage in populations at risk in these infections.

A question addressed by these studies is the nature of the transition state as substrates of differing nucleophilicity are involved in displacing nicotinamide. The results (Figure 16) indicate that the transition states for hydrolysis are similar for pH-independent hydrolysis (pH values from 3 to 7) and for the slow NAD^+ hydrolysis reactions catalyzed by all three enzymes when acceptor proteins are not present (107–110). In every case the ribosyl group has well-developed oxocarbenium ion character, with nearly full positive charge at the transition state. The attacking water nucleophile in all cases has a low bond order, more characteristic of a "spectator" nucleophile than one actively

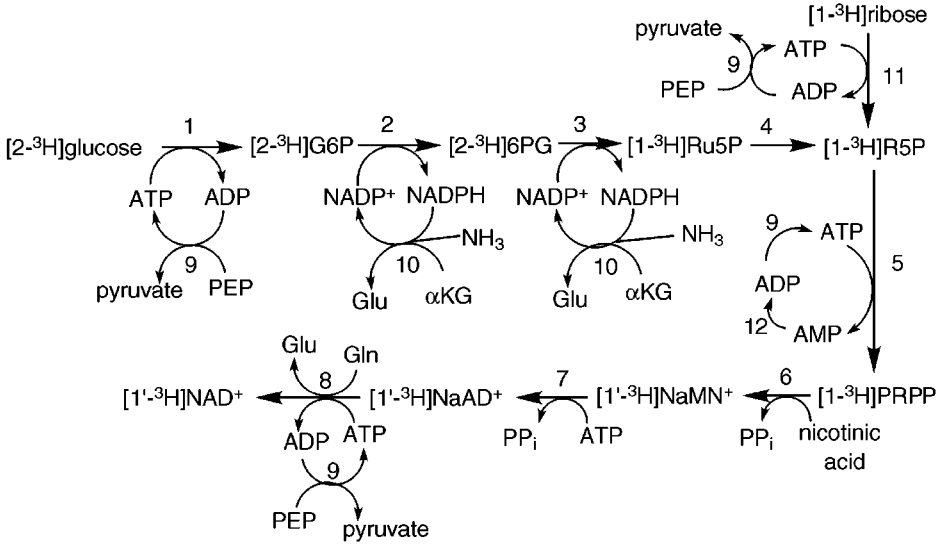

Figure 14 Enzymatic synthesis of specifically labeled NAD^+. Enzymes not identified in Figure 6 include 6 = nicotinate phosphoribosyl transferase, 7 = NAD^+ pyrophosphorylase, 8 = NAD^+ synthetase, and 11 = ribokinase.

participating in bond formation. However, the magnitude of the kinetic isotope effects requires a small degree of nucleophilic participation, less than 0.01 bond order at the transition state. The results establish that the water nucleophile does not play a role in forming the transition state, as occurs in nucleophilic displacement reactions. Rather, the enzymes catalyze formation of the ribooxocarbenium ion, and the neighboring water molecule then reacts with the electron-deficient center.

Transition state structures have been solved for pertussis toxin catalyzing the ADP-ribosylation of the C-terminal 20–amino acid peptide from $G_{i\alpha 3}$ and the G-protein $G_{i\alpha 1}$ (111, 112; Figure 16). In both cases, the ADP-ribosyl acceptor is a specific Cys sulfhydryl. The reaction for peptide ADP-ribosylation gave intrinsic kinetic isotope effects, and the transition state structure shows increased nucleophilic participation by the thiolate anion (Figure 16). Electrostatic potential surfaces of the transition state for ADP-ribosylation of a thiolate anion are shown in Figure 17 (color plate). In NAD^+ the positive charge is distributed nearly equally in the ribosyl and nicotinamide, giving rise to an elongated, weak N-ribosidic bond. At the transition state the leaving group is neutral and the full positive charge has migrated into the ribose. Attack by the thiolate anion neutralizes the oxocarbenium ion charge to form the ion-paired transition state (111).

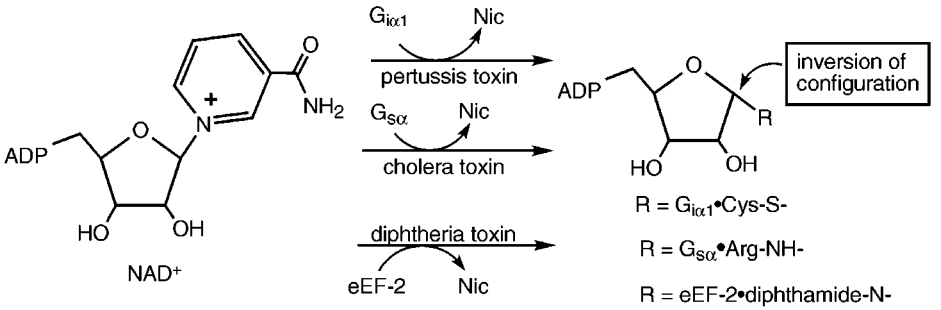

Figure 15 Reactions catalyzed by the ADP-ribosylating agents: pertussis toxin, cholera toxin, and diphtheria toxin. In the absence of the G-protein acceptors, all toxins catalyze the slow hydrolysis of NAD^+ to form nicotinamide (Nic) and ADP-ribose (where R = OH). All of the known ADP-ribosylation reactions involve inversion of configuration at C1′ of the ribosyl.

The ADP-ribosylation reaction for the protein $G_{i\alpha 1}$ involves the concerted interactions of the G protein, NAD^+, and pertussis toxin A-chain enzyme. To express intrinsic kinetic isotope effects, the chemical bond change must be the slowest step in the reaction. It was previously unknown whether protein covalent modifications could be investigated by kinetic isotope effect methods. Of concern were the slow conformational changes that dominate most protein-protein interactions and the potentially rate-limiting release of a protein product

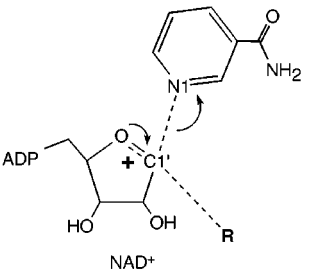

	bond order at transition state	
catalyst - reaction	C1'-N1	C1'-**R**
solvolysis	0.02	0.005
cholera-hydrolysis	0.11	0.002
pertussis-hydrolysis	0.11	0.001
diphtheria-hydrolysis	0.02	0.03
pertussis-peptide-ADPR	0.14	0.11
pertussis-$G_{i\alpha 1}$-ADPR	0.11	0.09

Figure 16 Summary of transition state structures for NAD^+ hydrolysis or ADP-ribosyl transfer. Solvolysis was at pH 4 in buffered H_2O. Hydrolysis by the three toxins is in the absence of ADP-ribose acceptors. For the pertussis-peptide-ADP-ribose (ADPR) reaction, the C-terminal 20–amino acid peptide from $G_{i\alpha 3}$ was used as the acceptor. Cys16 of the peptide is ADP-ribosylated. For the pertussis-$G_{i\alpha 1}$-ADPR reaction, purified recombinant $G_{i\alpha 1}$ was the acceptor and ADP-ribosylation occurs at a Cys located 4 amino acids from the C terminal of the protein.

from the catalytic site. Pertussis toxin binds tightly to the trimeric $\alpha\beta\gamma$-G-protein complex (0.8 μM K_m), but when $G_{i\alpha 1}$ is used alone, the K_m increases 1000-fold to 800 μM K_m with no change in k_{cat}, and intrinsic kinetic isotope effects are expressed (112). Similar methods may be applicable to other covalent modifications because the catalytic rates for covalent modifications are usually slow, a condition that favors expression of intrinsic kinetic isotope effects.

The site of ADP-ribosylation for pertussis toxin is a specific Cys residue located four amino acids from the C terminus of several G_i proteins. The attacking Cys thiol has been ionized to form the thiolate anion (RS^-) prior to reaching the transition state. Thiolate anions are efficient nucleophiles. As the enzyme converts NAD^+ to the enzyme-stabilized ribooxocarbenium ion, the juxtaposition of the thiolate results in a transition state with an increase in the bond order from the attacking nucleophile (Figure 16). The transition states increase in nucleophilic character when the physiological peptide substrates are present. This change is likely to reflect an ability of the enzyme to position the attacking thiolate nucleophile for optimum interaction as the ribooxocarbenium ion is formed.

Docking the NAD^+ hydrolytic transition state formed by diphtheria toxin into the X-ray crystal structure determined with NAD^+ in the catalytic site provides revealing information for the formation of the ribooxocarbenium transition state (Figure 17, color plate). The crystal structure of the Michaelis complex of diphtheria toxin-NAD^+ reveals the nicotinamide ring in a hydrophobic pocket (113). The ring is not inserted full depth into the pocket, and the essential catalytic site carboxylate, Glu148, is poorly positioned with respect to the ribooxocarbenium ion of the transition state. Removing NAD^+ from the crystal structure and replacing it with the transition state also provides poor enzymatic contacts. The ribooxocarbenium ion does not contact the protein until the nicotinamide group is inserted more deeply, about an additional 1 Å, into the hydrophobic pocket. Following this translation, the catalytic site Glu148 is well positioned to stabilize the positive charge that develops at C1′ in the transition state. The hydrophobic pocket is energetically unfavorable for the positive charge on the reactant nicotinamide and forces it toward the ribose, where it is accommodated in the oxocarbenium ion and stabilized by Glu148. Water is an inefficient nucleophile to attack the ribooxocarbenium ion, and hydrolysis occurs slowly. When the acceptor G protein is present, the reaction occurs more rapidly because the toxin ionizes the Cys ADP-ribosylation site to form the nucleophilic thiolate anion. These features of the transition state are adequate to predict the structure of stable compounds that mimic the transition state. It is hoped that this information will lead to new agents to intervene in these infections.

INHIBITOR PREDICTION FROM TRANSITION STATE INHIBITORS

Similarity Measures

A goal of transition state investigation has been to use the knowledge to design transition state inhibitors and to predict inhibitory strength. Transition states stabilized by enzymes bind strongly by virtue of their geometric and electrostatic fit to the enzyme conformation that stabilizes the unstable electronic structure. Geometric similarity of a transition state inhibitor is necessary to provide volumetric access to the catalytic site and to establish the correct distance to the enzymatic contacts. Electronic similarity is essential to make the correct H-bond, ionic, and hydrophobic contacts found in the transition state interaction. If every detail of the transition state structure could be reproduced in a stably bonded transition state analog, it would approach the transition state binding energy of 10^{10}–10^{15} times tighter than the substrate. Despite the problem of exact matching, striking similarity is apparent in molecular electrostatic potential surfaces of transition state structures and those of transition state inhibitors (Figure 10, color plate). It is possible to establish a predictive relationship between the binding affinity of an inhibitor and its similarity to the enzymatic transition state.

Prediction of Inhibitory Strength

Bagdassarian et al (114, 115) examined this relationship using three enzymes for which the transition state structures had been characterized by kinetic isotope effects. AMP deaminase, adenosine deaminase, and AMP nucleosidase were considered by comparing the geometric and molecular electrostatic potential surfaces of the experimentally determined transition states with the substrates and a series of inhibitors exhibiting classic competitive inhibition and slow-onset, tight-binding inhibition (e.g. 78). An algorithm was used that considers the electrostatic potential and its spatial distribution at the van der Waals surface of test inhibitors. These parameters were compared to those for the transition state structure, and an electronic similarity index (S_e) was assigned, with a value of 1.0 indicating a perfect match for molecular electrostatic potential (a molecule compared to itself gives $S_e = 1.0$). Comparison of the transition state S_e with those from substrate and inhibitors that bind better than substrate gave a strong correlation in electrostatic similarity and binding energy ($\Delta G/RT$) over a large range of binding energies encompassing the substrate and the transition state. Approaches that match the features of experimentally determined transition states to those of proposed inhibitors have substantial potential for the prediction of new inhibitors prior to synthetic efforts.

CONCLUSIONS

Experimental access to enzymatic transition state structures has provided novel information about the nature of catalysis. It is reasonable to anticipate that the continued application of this information will permit the design and synthesis of powerful transition state inhibitors that incorporate desired pharmacologic properties. The ability to solve transition state structures has been made possible only by the development of kinetic methods to establish the rate-limiting steps in reactions, synthetic methods for labeled compounds, and computational chemistry and theory to quantitate kinetic isotope effects and to predict electron distribution in partially bonded molecules. The next advance in this area will see these technologies applied to the development of new inhibitors.

ACKNOWLEDGMENTS

Preparation of this work and research in this laboratory have been made possible by the support of research and training grants from the National Institutes of Health, the United States Army, The G. Harold and Leila Y. Mathers Charitable Foundation, the American Cancer Society, and the National Sciences and Engineering Research Council (Canada). I thank Dr. Paul Berti for assistance in figure preparation.

Literature Cited

1. Radzicka A, Wolfenden R. 1995. *Science* 267:90–93
2. Glasstone S, Laidler KJ, Eyring HK. 1941. *The Theory of Rate Processes*. New York: McGraw-Hill
3. Pauling L. 1948. *Am. Sci.* 36:50–58
4. Wolfenden R. 1972. *Acc. Chem. Res.* 5:10–18
5. Wolfenden R. 1976. *Annu. Rev. Biophys. Bioeng.* 5:271–306
6. Morrison JF, Walsh CT. 1988. *Adv. Enzymol. Relat. Areas Mol. Biol.* 61:201–301
7. Radzicka A, Wolfenden R. 1995. *Methods Enzymol.* 249:284–312
8. Bigeleisen J, Mayer MG. 1947. *J. Chem. Phys.* 15:261–67
9. Bigeleisen J, Wolfsberg M. 1958. *Adv. Chem. Phys.* 1:15–76
10. Streitwiser A Jr, Jagow RH, Fahey RC, Suzuki S. 1958. *J. Am. Chem. Soc.* 80: 2326–32
11. Cleland WW, O'Leary MH, Northrop DB, eds. 1977. *Isotope Effects on Enzyme-Catalyzed Reactions*. Baltimore, MD: Univ. Park Press
12. Gandour RD, Schowen RL, eds. 1978. *Transition States of Biochemical Processes*. New York: Plenum
13. Northrop DB. 1981. *Annu. Rev. Biochem.* 50:103–31
14. Cook PF, Cleland WW. 1981. *Biochemistry* 20:1790–96
15. Cook PF, Oppenheimer NJ, Cleland WW. 1981. *Biochemistry* 20:1817–25
16. Cleland WW. 1982. *Methods Enzymol.* 87:625–41
17. Scharschmidt M, Fisher MA, Cleland WW. 1984. *Biochemistry* 23:5471–78
18. Bolin JT, Filman DJ, Matthews DA, Hamlin RC, Kraut J. 1982. *J. Biol. Chem.* 257:13650–62
19. Kimble E, Hadala J, Ludewig R, Peters P, Greenberg G, et al. 1995. *Inflamm. Res.* 44:S181–82
20. Kline PC, Schramm VL. 1993. *Biochemistry* 32:13212–19

21. Shan S-O, Herschlag D. 1996. *Proc. Natl. Acad. Sci. USA* 93:14474–79
22. Cleland WW, Kreevoy MM. 1994. *Science* 264:1887–90
23. Truhlar DG, Hase WL, Hynes JT. 1983. *J. Phys. Chem.* 87:2664–82
24. Albery WJ. 1993. *Adv. Phys. Org. Chem.* 28:139–70
25. Kurz LC, Weitkamp E, Frieden C. 1987. *Biochemistry* 26:3027–32
26. Frick L, Yang C, Marquez VE, Wolfenden R. 1989. *Biochemistry* 28:9423–30
27. Wilson DK, Rudolph FB, Quiocho FA. 1991. *Science* 252:1278–84
28. Warshel A. 1991. *Computer Modeling of Chemical Reactions in Enzymes and Solutions*. New York: Wiley & Sons
29. Cleland WW. 1977. *Adv. Enzymol. Relat. Areas Mol. Biol.* 45:273–387
30. Parkin DW, Schramm VL. 1995. *Biochemistry* 34:13961–66
31. Albery WJ, Knowles JR. 1977. *Angew. Chem.* 16:285–93
32. Schowen RL. 1978. In *Transition States of Biochemical Processes*, ed. RD Gandour, RL Schowen, pp. 77–114. New York: Plenum
33. Melander L, Saunders WJ Jr. 1980. *Reaction Rates of Isotopic Molecules*. New York: Wiley & Sons
34. Cleland WW. 1995. *Methods Enzymol.* 249:341–73
35. Jencks WP. 1987. In *Catalysis in Chemistry and Enzymology*, pp. 170–82. New York: Dover
36. Hammond GS. 1955. *J. Am. Chem. Soc.* 77:334–38
37. Agarwal RP, Spector T, Parks RE Jr. 1977. *Biochem. Pharmacol.* 26:359–67
38. Bachovin WW, Wong WYL, Farr-Jones S, Shenvi AB, Kettner CA. 1988. *Biochemistry* 27:12839– 46
39. Rodgers J, Femec DA, Schowen RL. 1982. *J. Am. Chem. Soc.* 104:3263–68
40. Schramm VL, Horenstein BA, Kline PC. 1994. *J. Biol. Chem.* 269:18259–62
41. Huskey WP. 1991. See Ref. 116, pp. 37–72
42. Suhnel J, Schowen RL. 1991. See Ref. 116, pp. 3–35
43. Cleland WW. 1987. *Bioorg. Chem.* 15: 282–302
44. Sunko DE, Szele I, Hehre WJ. 1977. *J. Am. Chem. Soc.* 99:5000–4
45. Bennet AJ, Sinnott ML. 1986. *J. Am. Chem. Soc.* 108:7287–94
46. Northrop DB. 1975. *Biochemistry* 14: 2644–51
47. Sims LB, Burton GW, Lewis DE. 1977. *BEBOVIB-IV, QCPE No. 337*. Bloomington, IN. Quantum Chem. Program Exch., Dep. Chem., Univ. Indiana
48. Sims LB, Lewis DE. 1984. In *Isotopes in Organic Chemistry*, ed. E Buncel, CC Lee, 6:161–259. New York: Elsevier
49. Stewart JJP. 1989. *Comput. Chem.* 10: 209–20
50. Frisch MJ, Trucks GW, Schlegel HB, Gill PMW, Johnson BG, et al. 1995. *Gaussian 94, Rev. C. 2, 1995*. Pittsburgh, PA: Gaussian Inc.
51. Schramm VL. 1976. *J. Biol. Chem.* 251: 3417–24
52. Schramm VL. 1974. *J. Biol. Chem.* 249: 1729–36
53. Leung HB, Schramm VL. 1984. *J. Biol. Chem.* 259:6972–78
54. Parkin DW, Leung HB, Schramm VL. 1984. *J. Biol. Chem.* 259:9411–17
55. Parkin DW, Schramm VL. 1987. *Biochemistry* 26:913–20
56. Mentch F, Parkin DW, Schramm VL. 1987. *Biochemistry* 26:921–30
57. Srinivasan K, Konstantinidis A, Sinnott ML, Hall BG. 1993. *Biochem. J.* 291:15–17
58. Pauling L. 1960. *The Nature of the Chemical Bond*. Ithaca, NY: Cornell Univ. Press. 3rd ed.
59. DeWolf WE Jr, Fullin FA, Schramm VL. 1979. *J. Biol. Chem.* 254:10868–75
60. Leung HB, Schramm VL. 1980. *J. Biol. Chem.* 255:10867–74
61. Giranda VL, Berman HM, Schramm VL. 1988. *Biochemistry* 27:5813–18
62. Ehrlich JI, Schramm VL. 1994. *Biochemistry* 33:8890–96
63. Leung HB, Schramm VL. 1981. *J. Biol. Chem.* 256:12823–29
64. Parkin DW, Mentch F, Banks GA, Horenstein BA, Schramm VL. 1991. *Biochemistry* 30:921–30
65. Parry RJ, Minta A. 1982. *J. Am. Chem. Soc.* 104:871–72
66. Markham GD, Hafner EW, Tabor CW, Tabor H. 1980. *J. Biol Chem.* 255:9082–92
67. Larsen TM, Laughlin LT, Holden HM, Rayment I, Reed GH. 1994. *Biochemistry* 33:6301–9
68. Markham GD, Parkin DW, Mentch F, Schramm VL. 1987. *J. Biol. Chem.* 262: 5609–15
69. Rose IW. 1980. *Methods Enzymol.* 64:47–59
70. Carey FA, Sundberg RF. 1990. *Advanced Organic Chemistry. Part A: Structure and Mechanism*, pp. 579–83. New York: Plenum. 3rd ed.
71. Merkler DJ, Wali AS, Taylor J, Schramm

VL. 1989. *J. Biol. Chem.* 264:21422–30
72. Lowenstein JM. 1972. *Physiol. Rev.* 52:382–414
73. Sabina RL, Holmes EW. 1995. See Ref. 117, pp. 1769–80
74. Xia Y, Khatchikian G, Zweier JL. 1996. *J. Biol. Chem.* 271:10096–102
75. Hershfield MS, Mitchell BS. 1995. See Ref. 117, pp. 1725–68
76. Frieden C, Kurz LC, Gilbert HR. 1980. *Biochemistry* 19:5303–9
77. Kati WM, Wolfenden R. 1989. *Science* 243:1591–93
78. Merkler DJ, Brenowitz M, Schramm VL. 1990. *Biochemistry* 29:8358–64
79. Merkler DJ, Kline PC, Weiss P, Schramm VL. 1993. *Biochemistry* 32:12993–3001
80. Weiss PM, Cook PF, Hermes JD, Cleland WW. 1987. *Biochemistry* 26:7378–84
81. Merkler DJ, Schramm VL. 1993. *Biochemistry* 32:5792–99
82. Kline PC, Schramm VL. 1994. *Biochemistry* 34:1153–62
83. Hammond DJ, Gutteridge WE. 1984. *Mol. Biochem. Parasitol.* 13:243–61
84. Parkin DW, Horenstein BA, Abdulah DR, Estupiñán B, Schramm VL. 1991. *J. Biol. Chem.* 266:20658–65
85. Estupiñán B, Schramm VL. 1994. *J. Biol. Chem.* 269:23068–73
86. Parkin DW. 1996. *J. Biol. Chem.* 271:21713–19
87. Horenstein BA, Parkin DW, Estupiñán B, Schramm VL. 1991. *Biochemistry* 30:10788–95
88. Pelle R, Schramm VL, Parkin DW. 1998. *J. Biol. Chem.* 273:2118–26
89. Horenstein BA, Schramm VL. 1993. *Biochemistry* 32:7089–97
90. Horenstein BA, Schramm VL. 1993. *Biochemistry* 32:9917–25
90a. Degano M, Almo SC, Sacchettini JC, Schramm VL. 1998. *Biochemistry.* In press
91. Horenstein BA, Zabinski RF, Schramm VL. 1993. *Tetrahedron Lett.* 34:7213–16
92. Boutellier M, Horenstein BA, Semenyaka A, Schramm VL, Ganem B. 1994. *Biochemistry* 33:3994–4000
93. Parkin DW, Schramm VL. 1995. *Biochemistry* 34:13961–66
94. Furneaux RH, Limberg G, Tyler PC, Schramm VL. 1997. *Tetrahedron* 53: 2915–30
95. Deng H, Chan AWY, Bagdassarian CK, Estupiñán B, Ganem B, et al. 1996. *Biochemistry* 35:6037–47
96. Markert ML, Finkel BD, McLaughlin TM, Watson TJ, Collard HR, et al. 1997. *Hum. Mutat.* 9:118–21
97. Kline PC, Schramm VL. 1992. *Biochemistry* 31:5964–73
98. Kline PC, Schramm VL. 1995. *Biochemistry* 34:1153–62
99. Goiten RK, Chelsky D, Parsons SM. 1978. *J. Biol. Chem.* 253:2963–71
100. Tao W, Grubmeyer C, Blanchard JS. 1996. *Biochemistry* 35:14–21
101. Scapin G, Grubmeyer C, Sacchettini JC. 1994. *Biochemistry* 33:1287–94
102. Scapin G, Ozturk DH, Grubmeyer C, Sacchettini JC. 1995. *Biochemistry* 34:10744–54
103. Bull HG, Ferraz JP, Cordes EH, Ribbi A, Apitz-Castro R. 1978. *J. Biol. Chem.* 253:5186–92
104. Ferraz JP, Bull HG, Cordes EH. 1978. *Arch. Biochem. Biophys.* 191:431–36
105. Rising KA, Schramm VL. 1994. *J. Am. Chem. Soc.* 116:6531–36
106. Moss J, Vaughan M, eds. 1990. *ADP-Ribosylating Toxins and G-Proteins. Insights into Signal Transduction.* Washington, DC: Am. Soc. Microbiol.
107. Rising KA, Schramm VL. 1997. *J. Am. Chem. Soc.* 119:27–37
108. Berti PJ, Schramm VL. 1997. *J. Am. Chem. Soc.* 119:12069–78
109. Scheuring J, Schramm VL. 1997. *Biochemistry* 36:4526–34
110. Berti PJ, Blanke SR, Schramm VL. 1997. *J. Am. Chem. Soc.* 119:12079–88
111. Scheuring J, Schramm VL. 1997. *Biochemistry* 36:8215–23
112. Scheuring J, Berti PJ, Schramm VL. 1998. *Biochemistry.* 37:2748–58
113. Bell CE, Eisenberg D. 1996. *Biochemistry* 35:1137–49
114. Bagdassarian CK, Braunheim BB, Schramm VL, Schwartz DD. 1996. *Int. J. Quantum Chem.* 60:73–80
115. Bagdassarian CK, Schramm VL, Schwartz SD. 1996. *J. Am. Chem. Soc.* 118:8825–36
116. Cook PF, ed. 1991. *Enzyme Mechanism from Isotope Effects*. Boca Raton, FL: CRC
117. Scriver CR, Beaudet AL, Sly WS, Valle D, eds. 1995. *The Metabolic and Molecular Basis of Inherited Disease*. New York: McGraw-Hill. 7th ed.

Annual Review of Biochemistry
Volume 67, 1998

CONTENTS